

Line emission from gamma-ray burst environments

Markus Böttcher^{1,2}

Submitted to the Astrophysical Journal

ABSTRACT

The time and angle dependent line and continuum emission from a dense torus around a cosmological gamma-ray burst source is simulated, taking into account photoionization, collisional ionization, recombination, and electron heating and cooling due to various processes. The importance of the hydrodynamical interaction between the torus and the expanding blast wave is stressed. Due to the rapid deceleration of the blast wave as it interacts with the dense torus, the material in the torus will be illuminated by a drastically different photon spectrum than observable through a low-column-density line of sight, and will be heated by the hydrodynamical interaction between the blast wave and the torus. A model calculation to reproduce the Fe K α line emission observed in the X-ray afterglow of GRB 970508 is presented. The results indicate that $\sim 10^{-4} M_{\odot}$ of iron must be concentrated in a region of $R \lesssim 10^{-3}$ pc. The illumination of the torus material due to the hydrodynamical interaction of the blast wave with the torus is the dominant heating and ionization mechanism leading to the formation of the iron line. These results suggest that misaligned GRBs may be detectable as X-ray flashes with strong emission line features.

Subject headings: Atomic processes — Radiative transfer — Gamma rays: bursts — X-rays: bursts

1. Introduction

The recent marginal detections of redshifted iron K α emission lines in the X-ray afterglows of GRB 970508 (Piro et al. 1999) and GRB 970828 (Yoshida et al. 1999) have stimulated vital interest in the processes of photoionization and fluorescence line emission in gamma-ray burst (GRB) environments as a potentially powerful tool for redshift measurements and mapping of the density structure and composition of the vicinity of cosmological GRBs. X-ray absorption features and fluorescence line emission from the environments of cosmological GRBs have been investigated theoretically by Mészáros & Rees (1998b), Böttcher et al. (1999a), Böttcher, Dermer & Liang

¹Chandra Fellow

²Department of Space Physics and Astronomy, Rice University, MS 108, 6100 S. Main St., Houston, TX 77005-1892

(1999b), and Ghisellini et al. (1999). These studies were motivated by suggestions that GRBs are caused by the death of a very massive star (Woosley 1993; Paczyński 1998; Stella & Vietri 1998) and are therefore likely to be embedded in the dense gaseous environment of a star-forming region. The *HST* image of the optical counterpart of the extremely bright GRB 990123 possibly provided the first direct observation of an association of a GRB with a star-forming region of the proposed host galaxy (Bloom et al. 1999a). (Note, however, that Holland & Hjorth [1999] have found that the optical counterpart is located at a distance of $\gtrsim 1.3$ kpc from the nearest star-forming region resolvable in the *HST* image of the host galaxy after subtraction of the optical transient, which is larger than the expected separation of a very massive star from its birth place.) Bloom et al. (1999a) have also demonstrated that those GRBs with optical afterglows and identification with a host galaxy are significantly offset from the centers of their host galaxies, but generally inside the galaxy’s effective radius. The possible association of GRB 980425 with the Type Ic supernova SN 1998bw (Galama et al. 1998) and the marginal evidence of a supernova underlying the optical light curve of GRB 980329 (Bloom et al. 1999b) provide further support for GRB source models related to the death of massive stars, at least for those $\sim 50\%$ of well-localized GRBs for which optical afterglows are observable and the correlation with host galaxies can be established.

For this reason, Ghisellini et al. (1999) and Böttcher et al. (1999a) have investigated the influence of a dense, quasi-isotropic GRB environment, as appropriate for a star-forming region, on the observable radiation, in terms of X-ray absorption features and fluorescence line emission. However, the results of Böttcher et al. (1999a, b) indicate that while a temporally varying Fe K absorption edge might be a powerful tool to gain information even about an isotropic GRB environment, the luminosity and duration of the Fe K α line observed in GRB 970508 (Piro et al. 1999), if real, is inconsistent with a quasi-isotropic environment. This is mainly because the column density of material along our line of sight toward the GRB is strongly constrained by the lack of detectable X-ray absorption features and by the requirement that the Thomson scattering optical depth τ_T along the line of sight must be $\tau_T \ll 1$ because otherwise the short-term variability of the burst radiation would be smeared out over the photon escape time scale from the environment.

A plausible way to solve this problem is the assumption of a strongly anisotropic GRB environment from which a GRB is only observed if we happen to look at the system through a line of sight with low absorption and Thomson depth. Such a geometry may be provided in the form of a dense torus surrounding the GRB source which could be produced by anisotropic ejecta of the burst progenitor, such as a dense stellar wind ejected by the progenitor of a hypernova (Paczyński 1998) or the remnant of a supernova preceding a supranova (Stella & Vietri 1998). That equatorial density enhancements around massive stars and supernova remnants may be a common phenomenon, is also supported by direct observations, e. g. of the bipolar structure of η Carinae (Davidson & Humphreys 1997) and the torus-shaped geometry visible in the *Chandra* image of this star³, the double ring structure of the remnant of SN 1987A, and the recent *Chandra*

³see <http://chandra.harvard.edu/photo/0099/index.html>

image of the central regions of the Crab nebula⁴.

An anisotropic geometry has recently been considered by Lazzati et al. (1999), who qualitatively discussed several relevant physical processes potentially leading to an observable Fe $K\alpha$ line in the X-ray afterglow of a GRB. The processes considered by these authors include (1) fluorescence line emission following multiple photoionization events, with the efficiency of line emission determined by the time scale for re-filling of the inner atomic shells of Fe by recombination in a very dense environment, (2) recombination and fluorescence line emission following electron-collisional ionization in a dense, hot plasma (called “thermal emission” in Lazzati et al. 1999), (3) fluorescence line emission in the course of reflection of the GRB radiation off a dense, highly opaque medium, in which most of the iron remains in a low ionization state. They find that the multiple-ionization – recombination scenario has problems due to the high electron temperature and implied long recombination times expected under the conditions where this process might be dominant, while their “thermal emission” and “reflection” scenarios appear more promising. Both processes require a very dense, highly opaque torus illuminated and heated by the GRB radiation. Thus, under these conditions, both processes might be important to a certain extent.

Recently, Weth et al. (2000) have studied the radiative response of an anisotropic GRB environment to the illumination by the prompt and afterglow radiation of the GRB, assuming that at any given point in time the radiation transport can be treated in thermal and ionization equilibrium, and that the blast wave associated with the GRB does not interact hydrodynamically with the dense material responsible for potentially observable absorption and emission features. In this approximation, they exploit a quasi-isotropic shell geometry and the geometry of an evacuated funnel, the walls of which act as a warm (partially ionized) Compton reflector. While the shell geometry was found to produce predominantly absorption features, followed by weaker line emission than observed in GRB 970508, the funnel geometry was appropriate to reproduce the observed Fe $K\alpha$ line from that burst.

In this paper, I present a detailed, time-dependent numerical study of the relevant processes in a dense torus illuminated by GRB radiation. The code used for this study originated from the time-dependent photoionization and line transfer code used in Böttcher et al. (1999a, b). The physics included in the numerical study is discussed in §2. In §3, general considerations and an appropriate model setup to reproduce the observed afterglow continuum of GRB 970508 (Piro et al. 1998,1999) are presented. General results of a parameter study, from which the required torus parameters necessary to reproduce the (marginally) detected Fe $K\alpha$ line in the X-ray afterglow of GRB 970508 (Piro et al. 1999) can be deduced, are discussed in §4. I summarize in §5.

⁴see <http://chandra.harvard.edu/photo/0052/index.html>

2. Model assumptions and computational scheme

In a previous paper (Böttcher et al. 1999a), we have investigated in detail the problem of time-dependent photoionization, photoelectric absorption and fluorescence line emission in the case of an isotropic, moderately dense GRB environment. Under the conditions investigated in that paper, recombination and electron-collisional effects were negligible and were thus not included in our treatment. In the situation investigated in this paper, such effects have to be considered carefully. Furthermore, the numerical problem is no longer isotropic. The code used in Böttcher et al. (1999a) has thus been modified in order to account for the anisotropy of the GRB environment.

The geometry assumed to treat this problem is illustrated in Fig. 1. The center of the coordinate system is the center of the GRB explosion. The GRB source is surrounded by a torus of dense material (particle density n_T), at a distance r_T from the center of the explosion. The radius of the cross-section of the torus is denoted by a . The burst source and the torus are embedded in a dilute ISM of density $n_{\text{ISM}}(r)$ which extends out to a radius r_{ISM} from the center of the explosion and is assumed to be distributed isotropically, but generally not homogeneously around the source.

The ISM and the torus are illuminated by the time-dependent radiation field of a GRB. The temporal evolution of the GRB radiation field is represented by the analytical expressions of Dermer, Chiang & Böttcher (1999), approximating the detailed predictions of external synchrotron shock model for GRBs (Rees & Mészáros 1992; Mészáros & Rees 1993; Katz 1994; Tavani 1996). The numerical scheme used to treat the time-dependent radiation transport problem is basically the same as described in Böttcher et al. (1999a), except that now the environment is anisotropic and more processes are included. The environment is split up in several (up to 22) angular zones, within which radial transfer of the GRB radiation is considered. To account for the anisotropy of the circumburster material (CBM), the expressions of Dermer et al. (1999) for the blast wave evolution need to be modified because the blast wave will be decelerated much more efficiently in the dense torus than in the dilute ISM. Each angular element of the CBM will be treated separately as if it were part of an isotropic, but inhomogeneous environment, characterized by a spherical shell of dense material of uniform density n_T extending from an inner radius r_1 to an outer radius r_2 (see Fig. 1). If the effect of blast wave deceleration in the dilute ISM prior to hitting the dense torus is negligible, the effective deceleration radius r_d will now be located at

$$r_d = \left(\frac{3 E_0}{4\pi n_T m_p c^2 \Gamma_0^2} + r_1^3 \right)^{1/3}, \quad (1)$$

where E_0 is the total energy of the primary ejecta in the spherical blast wave, Γ_0 is the bulk Lorentz factor of the material behind the shock front, and m_p is the proton mass. The deceleration of the blast wave may then be parametrized as a decrease of the bulk Lorentz factor Γ with radius r_b of the blast wave from the center of the explosion:

$$\Gamma(r_b) = \Gamma_0 \cdot \begin{cases} 1 & \text{if } r_b < r_d, \\ \xi^{-g} & \text{if } r_b \geq r_d, \end{cases} \quad (2)$$

where

$$\xi \equiv \left(\frac{r_b^3 - r_1^3}{r_d^3 - r_1^3} \right)^{1/3}. \quad (3)$$

The photon energy of the νF_ν spectrum will shift according to

$$\epsilon_p(r_b) = \epsilon_0 \left(\frac{n_T}{n_{\text{ISM}}} \right)^{1/2} \cdot \begin{cases} \text{const.} & \text{if } r_1 < r_b < r_d, \\ \xi^{-4g} & \text{if } r_b \geq r_d, \end{cases} \quad (4)$$

where ϵ_0 is the photon energy of the νF_ν spectrum at the peak of the burst in a direction where the blast wave only interacts with the dilute ISM. The νL_ν peak luminosity is

$$P_p(r_b) = 2\pi c \frac{2g-3}{g} \frac{m_p c^2 \Gamma_0^4 n_T}{(v^{-1} + \delta^{-1})} r_b^2 \cdot \begin{cases} \text{const.} & \text{if } r_1 < r_b < r_d, \\ \xi^{-4g} & \text{if } r_b \geq r_d, \end{cases} \quad (5)$$

where v and δ are the spectral indices, $\nu F_\nu \propto \epsilon^v$ below and $\nu F_\nu \propto \epsilon^{-\delta}$ above the peak photon energy, respectively.

Inspection of eqs. 1 – 5 shows that the interaction of the blast wave with the torus leads to an extremely short, extremely luminous flash of very high-energy radiation. The duration of this flash, as it would be measured by an observer located within or behind the torus, is given by

$$\Delta t_t = \frac{r_d - r_1}{2\Gamma_0^2 c} \approx \frac{E_0}{8\pi n_T m_p c^3 \Gamma_0^4 r_1^2} \approx 1.1 \times 10^{-5} \text{ s} \frac{E_{54}}{n_{10} \Gamma_{300}^4 r_{15}^2}, \quad (6)$$

where $E_{54} = E_0/(10^{54} \text{ ergs})$, $n_{10} = n_T/(10^{10} \text{ cm}^{-3})$, $\Gamma_{300} = \Gamma/300$, and $r_{15} = r_1/(10^{15} \text{ cm})$.

As the parts of the blast wave interacting with the torus are decelerated to subrelativistic velocities almost instantaneously, the material of the torus will be energized via shock heating and via photoionization by the X-ray and gamma-ray flash emitted during the phase of blast wave deceleration in the torus. The heating due to the subrelativistic shock is taken into account using basic energy and momentum conservation arguments. As has been argued by Vietri et al. (1999), the shock-heated torus material will attain a temperature of $\sim 3 \cdot 10^7 \text{ K}$, leading to strong Fe K α line emission via electron-impact ionization and subsequent recombination.

Line and continuum emission resulting from atomic processes in the ISM and the torus is assumed to be emitted isotropically at each point. The time delay (due to the light travel time difference) of such radiation reaching the observer from directions misaligned with respect to the line of sight to the GRB source, is properly taken into account. Since the column density of ISM and torus material along the line of sight as well as the light-travel-time delays depend on the

viewing angle, the output spectra and light curves are sampled under different viewing angles θ_{obs} with respect to the symmetry axis of the torus, which defines the z axis.

In addition to the processes of photoelectric absorption, photoionization and fluorescence line emission following photoionization events, which had been included already in Böttcher et al. (1999a), now radiative and dielectronic recombination, electron-collisional ionization, electron heating and cooling due to bremsstrahlung, Compton scattering, electron-impact ionization and Coulomb scattering, and continuum emission due to radiative recombination and bremsstrahlung emission are taken into account.

The radiative and dielectronic recombination rates are calculated using the results of Nahar & Pradhan (1997) for C and N, of Nahar (1999) for O, and of Nahar, Bautista & Pradhan (1997, 2000), Nahar (1996, 1997), and Nahar & Bautista (1999) for Fe I – V. The recombination rates for C-like ions are taken from Nahar (1995), and for Si-like ions from Nahar (2000). For the remaining iron ions, we use the tables of Arnaud & Raymond (1992). For ions in the He, Li, Be, and Ne isoelectronic sequences and not covered by the above references, we use the recombination rates of Romanik (1988). For the remaining ions, we use the coefficients given by Aldrovandi & Péquignot (1973), and Shull and van Steenberg (1982). A few subroutines of the XSTAR code (Kallman & McCray 1982) have been used. In addition to the corrections published in the Erratum to Shull and van Steenberg (1982), the following entries of their table 2 need to be corrected (Shull 1999, private communication): $A_{\text{di}}(\text{Si IX}) = 4.25 \cdot 10^{-2}$, $A_{\text{rad}}(\text{Si XI}) = 1.20 \cdot 10^{10}$, $A_{\text{di}}(\text{Ca IX}) = 4.02 \cdot 10^{-2}$, $A_{\text{rad}}(\text{Ca XI}) = 8.51 \cdot 10^{-11}$, $T_0(\text{Fe XVI}) = 8.18 \cdot 10^6$, $T_1(\text{Fe XXIV}) = 1.17 \cdot 10^7$. The rates of recombination into excited states are calculated using the hydrogenic approximation (Seaton 1959). 133 strong UV and X-ray lines due to radiative transitions following recombination into excited states been included using the line energies and branching ratios given by Kato (1976).

Due to the very high Compton equilibrium temperatures in the GRB surroundings, collisional ionization will largely dominate over collisional excitation so that excited states will be only weakly populated. Thus, for ease of computation, only photoionization from atoms and ions in the ground state is included.

The temperature of free electrons is determined by the excess energy of ionizing photons, the average energy of Auger electrons as given by Kaastra & Mewe (1993), Compton heating/cooling, Coulomb interactions with cold protons (using the prescription of Dermer & Liang [1989]) and bremsstrahlung and collisional ionization energy losses.

The electron-collisional ionization rates are calculated using the prescription of Shull & van Steenberg (1982). The standard formula for electron-ion bremsstrahlung emission (Rybicki & Lightman 1979) and the expression of Tucker & Koren (1971) for recombination continuum emission are used.

The elements included in the simulations are H, He, C, O, Ne, Mg, Si, S, Ca, Fe, and Ni since these are the most abundant elements in astrophysical plasmas, for which the relevant atomic data are readily available in the literature. The contributions from other elements have been neglected.

For the dilute surroundings of the GRB source, standard solar-system abundances, from Zombeck (1990), are assumed. Normalized to 1, the relative abundances are 0.935 (H), 6.33×10^{-2} (He), 3.90×10^{-4} (C), 8.12×10^{-5} (N), 6.47×10^{-4} (O), 9.14×10^{-5} (Ne), 3.73×10^{-5} (Mg), 3.52×10^{-5} (Si), 1.76×10^{-5} (S), 3.73×10^{-6} (Ar), 2.20×10^{-6} (Ca), 3.16×10^{-5} (Fe), 1.68×10^{-6} (Ni).

The chemical composition of the material in the torus is dominated by the ejecta of the GRB progenitor. The association of GRB 980425 with the type Ic SN 1998bw suggests that this material may be similar in composition to the ejecta of SN Ic's. These are probably related to core-collapse events and are known to be hydrogen- and helium deficient, i.e. their metal content is enhanced. Strong iron emission features in the early optical spectra, near the peak of the light curve, of this type of supernovae might indicate that in particular the iron abundance is significantly higher than in ordinary stellar atmospheres or in the ISM. Since very little is known about the actual relative element abundances in the ejecta, and the current X-ray data of GRB afterglows do not allow a composition analysis from the observational point of view, I will assume that the torus material has a tenfold iron overabundance with respect to the abundances quoted above, unless explicitly stated otherwise.

3. Model setup for GRB 970508

GRB 970508 was a moderately bright burst with a peak flux of $\Phi_p \approx 3.4 \cdot 10^{-7}$ ergs cm s⁻² and a duration of $t_\gamma \approx 15$ s in the energy band of the GRBM on board the *BeppoSAX* satellite (40 – 700 keV). The X-ray flux measured by the WFC of *BeppoSAX* exhibits a power-law decay ($F_\nu(t) \propto t^{-\chi}$) with index $\chi = 1.17 \pm 0.1$, until the time of a secondary X-ray outburst at $t \sim 6 \cdot 10^4$ s after the GRB (Piro et al. 1998). Piro et al. (1999) have recently reported the marginal detection of a possible Fe K α line with a line flux of $\Phi_L = (5 \pm 2) \cdot 10^{-5}$ cm⁻² s⁻¹ at the likely redshift of the burst, $z = 0.835$ (Metzger et al. 1997), during the first segment of the first period of observation by the NFI of *BeppoSAX* ($2.0 \cdot 10^4$ s – $5.6 \cdot 10^4$ s from the burst trigger time). The end point of this time slot was chosen as the onset of the secondary X-ray outburst.

When estimating the efficiency of reprocessing the illuminating GRB flux into Fe K α line flux and thus estimating the amount of mass required to produce the observed fluorescence line, it is important to take the effects of anisotropy of the CBM into account, as described in the previous section. If the density anisotropy due to the torus is strong, the assumption of the dense torus being illuminated and photoionized by radiation with the observed GRB characteristics will obviously yield a completely unrealistic picture, unless the blast wave is significantly decelerated by the more dilute material inside the radius of the torus before interacting with the torus. The latter condition would be equivalent to the torus being located outside the deceleration radius of the blast wave in the dilute external medium, i.e. $r_T \gg r_d^{\text{ISM}} = [3 E_0 / (4\pi n_{\text{ISM}} \Gamma_0^2 m_p c^2)]^{1/3} = 1.2 \times 10^{17} [E_{54} / (n_0 \Gamma_{300}^2)]^{1/3}$ cm, where $n_0 = n_{\text{ISM}} / (1 \text{cm}^{-3})$. If this is not the case, the material in the dense torus is expected to be illuminated by radiation, the photon spectrum and temporal evolution of which is drastically

different from the observed GRB spectrum. This is obvious from Eqs. 1 to 6. Although in this paper the external shock model is used to parametrize the GRB radiation and blast wave evolution, the same conclusions are true for an internal shock model for the prompt GRB radiation.

The duration of the observed line emission is most probably dominated by light-travel time effects rather than the intrinsic time scale of one of the physical process involved, such as recombination or electron-collisional ionization in a hot plasma, if the GRB and its afterglow are related to a relativistically expanding blast wave. This is because any point at a distance $R = 10^{16} R_{16}$ cm from the center of the burst source will either be swept up by the blast wave soon after the first light front of the GRB has reached it, or the blast wave will be effectively stopped before it reaches this point. During the coasting phase of the blast wave evolution, it is only illuminated for a time period

$$t_{ill} = \frac{R}{\beta_{\Gamma} c} (1 - \beta_{\Gamma}) \approx 1.9 \frac{R_{16}}{\Gamma_{300}^2} \text{ s}, \quad (7)$$

where $\beta_{\Gamma} = \sqrt{1 - \Gamma^{-2}}$. On the other hand, if this segment of the GRB environment is misaligned with respect to our line of sight to the GRB, then any isotropically emitted radiation from there will reach the observer with a time delay $\Delta t \sim R/c \sim 3 \cdot 10^5 R_{16} \text{ s} \gg t_{ill}$.

A pessimistic estimate of the necessary mass is based on the result of Böttcher et al. (1999a) that out to a radius of $R \sim 10^{20} (n_{\Gamma}[\text{cm}^{-3}])^{-1/3}$ cm iron in the CBM will be completely ionized. In a scenario in which the density of the illuminated material is relatively low so that recombination is negligible, the Fe $K\alpha$ line can only be emitted via fluorescence. Taking into account the large number of Auger electrons ejected following photoionization of iron in low ionization states, a fiducial number of $K\alpha$ line photons in the energy range 6.4 – 6.7 keV emitted in the course of complete ionization of an iron atom is ~ 5 since it takes on average ~ 12 X-ray photons to ionize an initially neutral Fe atom completely (Weisheit 1974), and the $K\alpha$ fluorescence yields for the various Fe ions are typically in the range 0.3 – 0.4. Thus, for a line luminosity $L_{K\alpha} = 10^{44} L_{44} \text{ ergs s}^{-1}$ emitted over a time scale $\Delta t_L = 10^5 t_5$ s, a total of

$$N_{\text{Fe}} = 2 \cdot 10^{56} \frac{L_{44} t_5}{f} \quad (8)$$

iron atoms is needed, where $f \geq 1$ is a correction factor accounting for the enhancement of the efficiency of line emission due to recombination and electron-collisional ionization. Eq. 8 yields a required mass of iron of

$$M_{\text{Fe}} = 0.16 \frac{L_{44} t_5}{f} M_{\odot}. \quad (9)$$

The line flux measured in the afterglow of GRB 970508 leads to an estimated mass of $M_{\text{Fe}} \sim 1 M_{\odot}$ of iron, concentrated in a region of $\lesssim 10^{-3}$ pc, which is highly unlikely to be realized in any known and well-understood astrophysical environment.

Assuming a dominant role of the effects of recombination and electron-impact ionization, one finds a more realistic lower limit on the required iron mass of $M_{\text{Fe}} \gtrsim 6 \cdot 10^{-6} M_{\odot}$ (Lazzati et al. 1999). It may thus be concluded that the effects of recombination and collisional ionization are dominant in the formation of the Fe K α line in GRB afterglows. In order for recombination to be efficient, the recombination time scale of iron needs to be $t_{\text{rec}} \ll 10^5$ s. Assuming temperatures of $T \sim 10^7 - 10^8$ K of the torus material, the typical recombination coefficients of highly ionized iron ions are $\alpha_{\text{rec}} \sim 10^{-11} \text{ cm}^3 \text{ s}^{-1}$, which implies that the density of material in the torus must be $n_T \gg 10^6 \text{ cm}^{-3}$.

In the framework of the analytical representation of Dermer et al. (1999), the spectral and temporal properties of GRB 970508 can be reasonably well reproduced assuming a total energy of the explosion of $\partial E/\partial\Omega = 3.6 \cdot 10^{52} \text{ ergs/sr}$, an initial bulk Lorentz factor of $\Gamma_0 = 100$, a uniform density of the ISM of $n_{\text{ISM}} = 4.8 \cdot 10^5 \text{ cm}^{-3}$, an equipartition factor $q = 8.15 \cdot 10^{-5}$, a quasi-adiabatic blast wave with $g = 1.6$ (the blast wave slows down as $\Gamma(r) \propto r^{-g}$ outside the deceleration radius), a low-energy spectral index (photon number index) of $\alpha_{\text{le}} = 2/3$ and a high-energy index of $\alpha_{\text{he}} = 2.1$. These parameters yield a deceleration time scale (which may be identified with the burst duration at γ -ray energies) of $t_d = 15$ s and a temporal decay of the X-ray afterglow with index $\chi = 1.2$. The peak of this model νF_{ν} spectrum during the prompt GRB phase is at $E_{\text{pk}} = 45$ keV, and its isotropic νL_{ν} peak luminosity at this photon energy is $2.8 \cdot 10^{50} \text{ ergs s}^{-1}$. All these features of the model GRB spectrum and spectral evolution are in good agreement with the observed properties of GRB 970508 (Piro et al. 1998). Obviously, the secondary X-ray flare at $t \approx 6 \cdot 10^4$ s is not modelled with this approach.

According to the synchrotron-shock model, the temporal decay index χ of the X-ray afterglow (produced by strongly cooled electrons behind the shock) is related to the radiative-regime parameter g , the decay index η of the external matter density ($n_{\text{ISM}} \propto r^{-\eta}$), and the high-frequency νF_{ν} spectral index $\delta = \alpha_{\text{he}} - 2$ through

$$\chi = \frac{4g(1 + \delta) + \eta(1 + \delta/2) - 2}{2g + 1} \quad (10)$$

(Dermer et al. 1999). Solving this for η , inserting $\chi = 1.17$, keeping in mind that $g \geq 1.5$, and assuming $\delta > 0$, we find that the external matter density gradient can not be steeper than $\eta \leq 0.68$. This means that within the framework of the standard synchrotron-shock model, the observed afterglow can not have been produced in an isotropic stellar-wind environment of the putative stellar progenitor, for which one would generally expect an r^{-2} density profile.

In the simulations presented here, the GRB explosion is allowed to be intrinsically anisotropic. In order not to introduce an uncontrollably large parameter space, only the effects of an angle-dependent energy output $(\partial E/\partial\Omega)(\theta)$ and baryon loading (or, equivalently, bulk Lorentz factor) $\Gamma(\theta)$ are investigated in this paper.

4. Results

In the first step, a series of simulations with intrinsically isotropic blast waves as specified in the previous section has been carried out in order to specify appropriate torus parameters to produce an iron line luminosity of $\sim 10^{44}$ ergs/s. In all simulations shown here, the torus is assumed to have an average distance of $r_T = 7 \cdot 10^{-4}$ pc from the center of the explosion in order to produce the observed time delay of the iron line emission with respect to the prompt GRB phase. As motivated in §2, the material in the torus has a tenfold overabundance of iron with respect to standard solar-system abundances, which are assumed for the surrounding ISM.

Fig. 2 illustrates the dependence of the produced iron line on the density of torus material, while the total mass of material in the torus is held constant (i.e. $a \propto n_T^{-1/2}$). The iron line intensity is strongly positively correlated with the density, which indicates the dominance of the density-dependent processes like electron-impact ionization and recombination in the formation of the line. Given a total torus mass of $M_T \lesssim 1 M_\odot$ and the assumed tenfold iron overabundance, a density of $n_T \gtrsim 10^{12} \text{ cm}^{-3}$ is necessary to produce the observed Fe $K\alpha$ line intensity. The figure also shows that the duration of the flash of iron line emission is determined by light travel time effects rather than the time scale of elementary processes because due to the high densities in the torus the recombination and collisional ionization time scales are $\ll 10^4$ s and thus shorter than the light travel time through the torus itself.

In Fig. 3, the effects of an intrinsically anisotropic blast wave are illustrated. In accord with the previous result that it is mainly electron-impact ionization and recombination which is responsible for the iron line emission, the effect of a limited amount of intrinsic anisotropy of the blast wave are only minor, as long as $[\partial E/\partial\Omega(\text{torus})] \gtrsim 0.01[\partial E/\partial\Omega(\text{l.o.s.})]$ and $\Gamma \gtrsim 30$. This is because the torus material rapidly becomes highly ionized and cools down to temperatures favorable for the production of an Fe $K\alpha$ line on time scales of $\ll 10^4$ s, only weakly dependent on the actual amount of energy deposited and on the detailed spectral characteristics of the illuminating radiation. The simulations show that the material ahead of the non-relativistic shock wave propagating through the torus is efficiently heated by the intense X-ray and gamma-ray flash produced during the initial deceleration of the blast wave within the torus. In these simulations, $[\partial E/\partial\Omega(\text{torus})] < [\partial E/\partial\Omega(\text{l.o.s.})]$ with $\Gamma_{\text{torus}} = \Gamma_{\text{l.o.s.}}$ corresponds to a smaller amount of mass ejected in the direction of the torus than along the evacuated funnel which points towards the observer. The case $\Gamma_{\text{torus}} < \Gamma_{\text{l.o.s.}}$ with $[\partial E/\partial\Omega(\text{torus})] = [\partial E/\partial\Omega(\text{l.o.s.})]$ corresponds to a higher baryon contamination in the direction of the torus.

Fig. 4 shows the result of a simulation which yields a reasonable representation of the afterglow spectrum of GRB 970508. Panel 4a shows the angle-dependent apparent luminosity of the Fe $K\alpha$ line compared to the luminosity in two continuum energy bands as a function of time. Panel 4b shows the simulated energy spectra at 3 different times for an observer located on the symmetry axis. The simulation predicts that the Fe $K\alpha$ line emission is only emitted in a rather short flash of a few times 10^4 s if the burst is observed close to the symmetry axis of the system.

Note that the absorption features visible in Fig. 4 are due to the influence of the ISM rather than the torus. However, as has been shown by Böttcher et al. (1999a) fluorescence line emission associated with this photoelectric absorption within the quasi-isotropic ISM may emerge above the background of the afterglow continuum only several weeks or months after the burst and is expected to have too low a flux level to be observable by any existing or currently planned X-ray telescope.

The actual composition of the material in the torus is rather uncertain. Fig. 5 illustrates how the predicted light curves and time-dependent X-ray spectra change for different He/H ratios and metal enhancement properties. The dotted curves show a test case with a He/H ratio of 0.2 (compared to the default value of 0.07), while the dot-dashed curves illustrate a case in which the abundances of all metals (i.e. all elements heavier than helium) is enhanced by a factor of 10. The expected equivalent width of the Fe $K\alpha$ line depends only weakly on the He/H ratio through the slightly higher electron density (and thus higher electron-impact ionization rate) in the helium-enhanced, highly ionized torus with respect to the standard He/H ratio. However, this also leads to more intense bremsstrahlung and radiative-recombination continuum emission from the hot, highly ionized torus, which shows up at energies \lesssim a few keV. Since this radiation propagates toward the observer through already highly ionized portions of the ISM, this continuum emission from the torus leads to an apparent weakening of the absorption features imprinted onto the afterglow radiation by the ISM.

An overabundance of all metals in the torus material (see dot-dashed curves in Fig. 5), leads to generally stronger emission line features around $t \sim 6 \times 10^4$ s. In addition to the Fe $K\alpha$ line, now also a weak Ni $K\alpha$ line at 7.5 – 7.7 keV and weak $K\alpha$ fluorescence and recombination lines from sulfur (2.3 – 2.4 keV), silicon (1.7 – 1.8 keV), and magnesium (\sim 1.3 keV), and an Fe L fluorescence line at \sim 0.7 keV become visible in the spectrum for a period of a few $\times 10^4$ s.

5. Summary and conclusions

I have presented results of a detailed numerical study of a scenario in which a relativistic blast wave associated with a cosmological gamma-ray burst irradiates and interacts with a torus of dense, metal-enriched material surrounding the burst source. The effects of photoionization, fluorescence line emission, recombination, electron-impact ionization, bremsstrahlung, Compton scattering, Coulomb scattering, and the hydrodynamical interaction of the blast wave with the torus have been considered. The effects of variations of several model parameters have been investigated, and a model calculation to reproduce the marginal detection of an Fe $K\alpha$ line in the X-ray afterglow of GRB 970508 has been presented.

The results indicate that in order to reproduce the observed iron line in the afterglow of GRB 970508 (if real), an iron mass of $\sim 10^{-4} M_{\odot}$ is required to be concentrated in a region of dense ($n_T \gtrsim 10^{12} \text{ cm}^{-3}$) material. The line is predominantly produced by electron-impact ionization and

recombination in the hot ($T \sim 10^8$ K), highly ionized torus. In order to give a realistic description of the model scenario investigated here, it is important to consider the effect of the anisotropy of the GRB environment on the radiation effectively illuminating the dense material. Unless the blast wave is substantially decelerated by the dilute ISM before interacting with the torus, the spectrum and spectral evolution of the illuminating radiation will be drastically different for the torus material with respect to the observed characteristics of the GRB and afterglow radiation.

The amount of line emission is rather weakly dependent on the He/H ratio in the torus material. However, significant deviations in the abundances of heavier elements from the standard solar-system values could be detectable through the respective fluorescence and recombination lines from these elements.

Given the limited significance of the detections of the iron lines in both the afterglows of GRB 970508 and GRB 970828, rapid follow-up observations by more sensitive X-ray telescopes with high spectral resolution are necessary to confirm the reality of these spectral features. Modern X-ray satellites like *Chandra* and *XMM* will be able to perform these observations with unprecedented sensitivity and spectral resolution. In case of positive detections, these X-ray line emission and absorption features may be an extremely powerful tool for redshift measurements and probing the environments of cosmological GRBs. This could ultimately help to distinguish between the two basic classes of GRB progenitor models, i.e. models related to the deaths of supermassive stars versus models involving the mergers of compact objects.

An interesting conclusion from these simulations is that X-ray flashes due to bremsstrahlung and radiative recombination continuum radiation from the dense, shock-heated torus should occasionally be observable even if the GRB itself is misaligned with respect to the observing direction. Such X-ray flashes with strong Fe $K\alpha$ line features may be hard to detect in archival data from, e. g., *ASCA* or *BeppoSAX*, but the increased sensitivity and imaging capability of *XMM* and *Chandra* may enable their detection.

The work of M.B. is supported by NASA through Chandra Postdoctoral Fellowship Award Number PF 9-10007, issued by the Chandra X-ray Center, which is operated by the Smithsonian Astrophysical Observatory for and on behalf of NASA under contract NAS 8-39073. I thank J. M. Shull for communicating the corrected values of the recombination rate coefficients to me, and E. P. Liang for stimulating discussions and careful reading of the manuscript. I also thank the anonymous referee for a very detailed review and many useful comments.

REFERENCES

- Aldrovandi, S. M. V., & Péquignot, D., 1973, *A&A* 25, 137; erratum: *A&A*, 47, 321 (1976)
Arnaud, M., & Raymond, J., 1992, *ApJ*, 398, 394

- Bloom, J. S., et al., 1999, *ApJ*, 518, L1
- Bloom, J. S., et al., 1999, *Nature*, 401, 453
- Böttcher, M., Dermer, C. D., Crider, A. W., & Liang, E. P., 1999a, *A&A*, 343, 111
- Böttcher, M., Dermer, C. D., & Liang, E. P., *A&AS*, 138, 543
- Davidson, K., & Humphreys, R. M., 1997, *ARAA*, 35, 1
- Dermer, C. D., Chiang, J., & Böttcher, M., 1999, *ApJ*, 513, 656
- Dermer, C. D., & Liang, E. P., 1989, *ApJ*, 339, 512
- Galama, T., et al., 1998, *Nature*, 395, 670
- Ghisellini, G., Haardt, F., Campana, S., Lazzati, D., & Covino, S., 1999, *ApJ*, 517, 168
- Holland, S., & Hjorth, J., 1999, *A&A*, 344, L67
- Kaastra, J. S., & Mewe, R., 1993, *A&AS*, 97, 443
- Kallman, T. R., & McCray, R. A., 1982, *ApJS*, 50, 263
- Kato, T., 1976, *ApJS*, 30, 397
- Katz, J. I., 1994, *ApJ*, 432, L107
- Lazzati, D., Campana, G., & Ghisellini, G., 1999, *MNRAS*, 304, L31
- Mészáros, P., & Rees, M. J., 1993, *ApJ*, 405, 278
- Mészáros, P., & Rees, M. J., 1998a, *ApJ*, 502, L105
- Mészáros, P., & Rees, M. J., 1998b, *MNRAS*, 299, L10
- Metzger, M. R., et al., 1997, *Nature*, 387, 878
- Nahar, S. N., 1995, *ApJS*, 101, 423 (Erratum: *ApJS*, 106, 213)
- Nahar, S. N., 1996, *Phys. Rev. A*, 53, 2417
- Nahar, S. N., 1997, *Phys. Rev. A*, 55, 1980
- Nahar, S. N., 1999, *ApJS*, 120, 131
- Nahar, S. N., 2000, *ApJS*, in press
- Nahar, S. N., & Bautista, M. A., 1999, *ApJS*, 120, 327
- Nahar, S. N., Bautista, M. A., & Pradhan, A. K., 1997, *ApJ*, 479, 497

- Nahar, S. N., Bautista, M. A., & Pradhan, A. K., 2000, *Phys. Rev. A*, in press
- Nahar, S. N., & Pradhan, A. K., 1997, *ApJS*, 111, 339
- Paczyński, B., 1998, *ApJ*, 494, L45
- Piro, L., et al., 1998, *A&A*, 331, L41
- Piro, L., et al., 1999, *ApJ*, 514, L73
- Rees, M. J., & Mészáros, P., 1992, *MNRAS*, 258, 41P
- Rybicki, G. B., & Lightman, A. P., 1979, “Radiative Processes in Astrophysics”, John Wiley & Sons
- Seaton, M. J., 1959, *MNRAS*, 119, 81
- Shull, J. M., & van Steenberg, M., 1982, *ApJS*, 48, 95 (Erratum: *ApJS*, 49, 351 [1982])
- Stella, L., & Vietri, M., 1998, *ApJ*, 507, L45
- Tavani, M., 1996, *Phys. Rev. Letters*, 76, 3478
- Tucker, W. H., & Koren, M., 1971, *ApJ*, 168, 283
- Vietri, M., Perola, C., Piro, L., & Stella, L., 1999, *MNRAS*, 308, L29
- Weisheit, J. C., 1974, *ApJ*, 190, 735
- Weth, C., Mészáros, P., Kallman, T., & Rees, M. J., 2000, *ApJ*, in press (astro-ph/9908243)
- Woosley, S. E., 1993, *ApJ*, 405, 273
- Yoshida, A., et al., 1999, *A&AS*, 138, 433
- Zombeck, M. V., 1990, “Handbook of Space Astronomy & Astrophysics”, Cambridge University Press

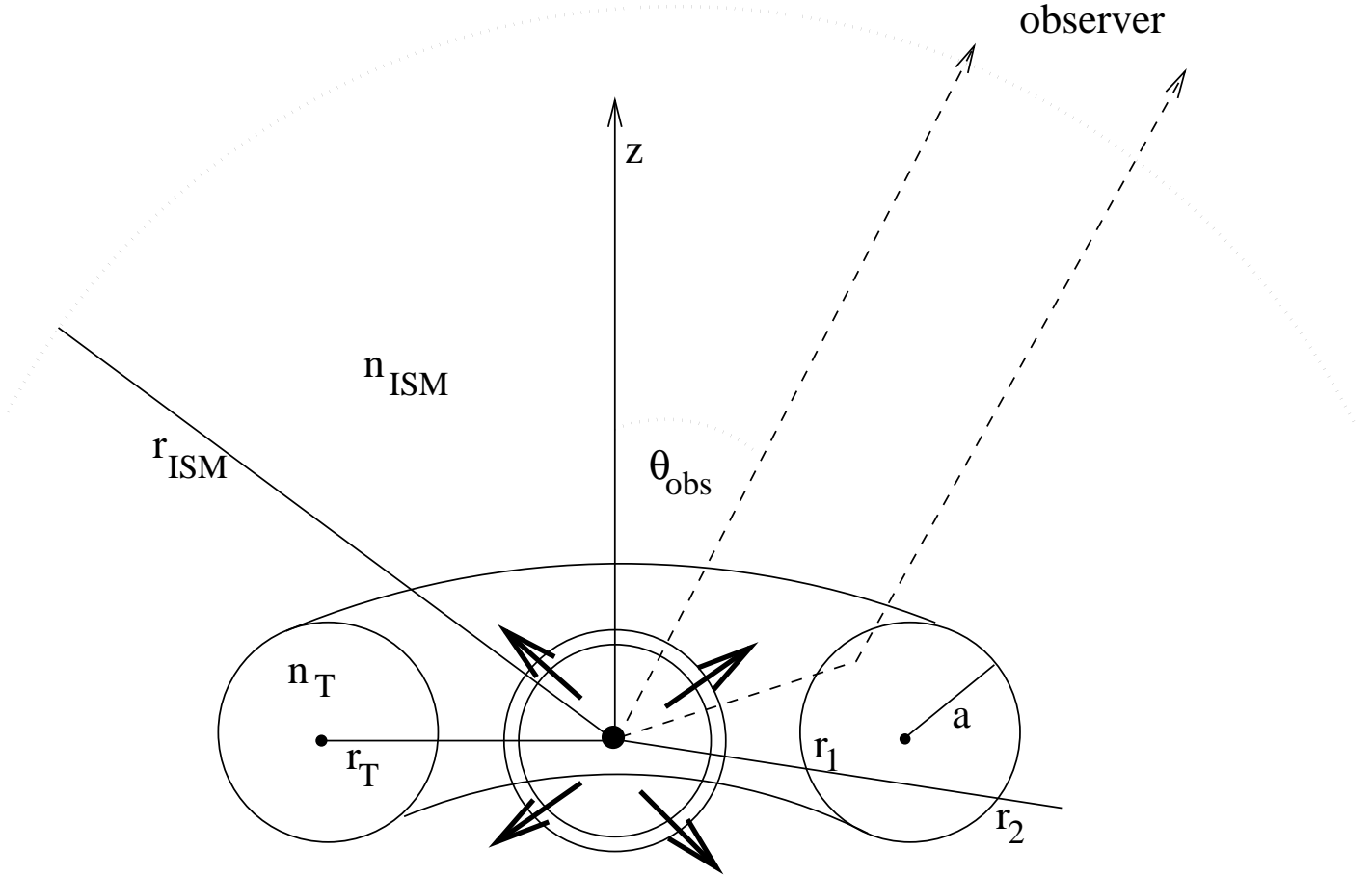


Fig. 1.— Illustration of the model geometry: A relativistic blast wave, initiated at the origin, interacts with the surrounding medium and emits the observable GRB and afterglow radiation. The burst source is surrounded by a torus of dense, metal enriched material at a distance r_{T} from the center of the explosion. a is the cross-sectional radius of the torus. The entire configuration is embedded in a homogeneous ISM with density n_{ISM} and standard solar-system element abundances.

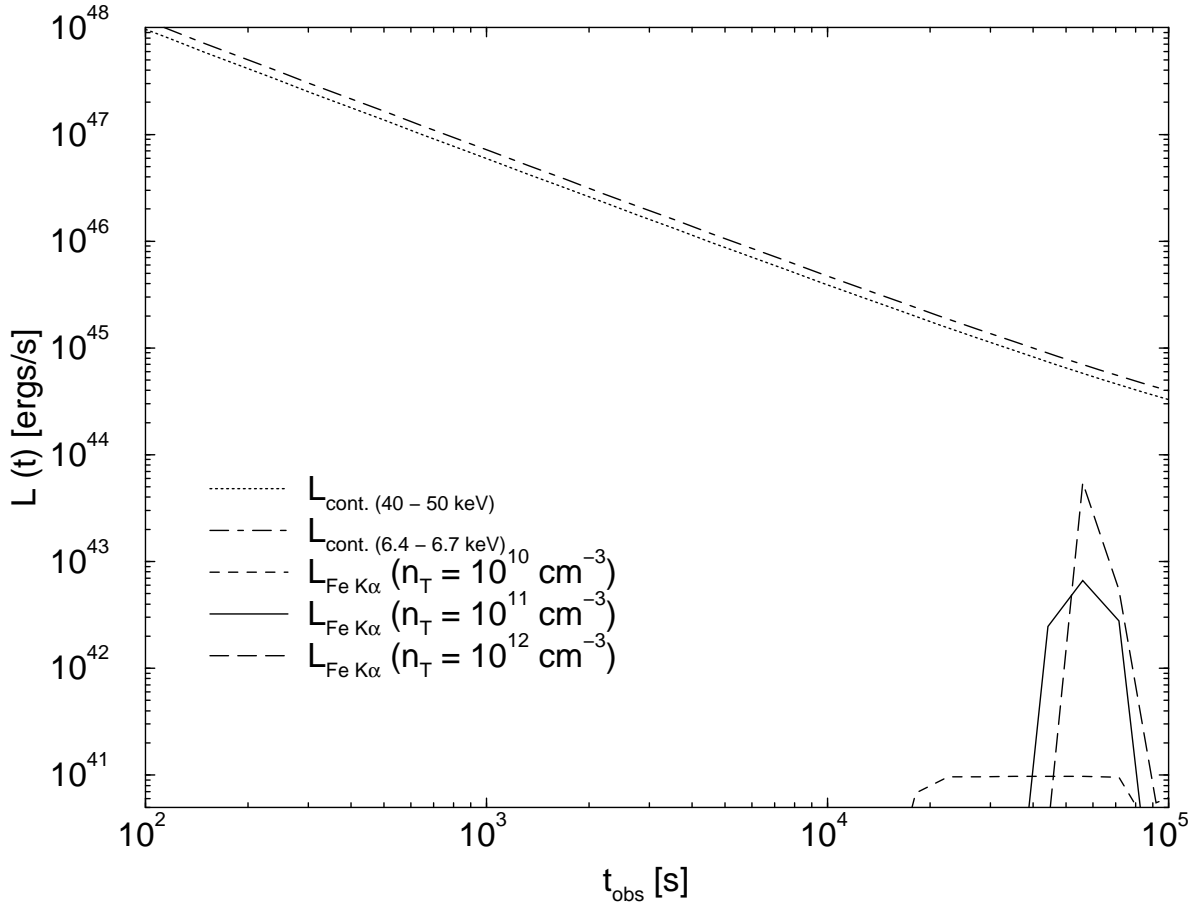


Fig. 2.— Light curves of the apparent isotropic luminosity in two continuum energy bands (dotted and dot-dashed curves, respectively) and in the Fe K α line for three different values of the density n_{T} of torus material. All other parameters are fixed (see text). The blast wave is assumed to be intrinsically isotropic; the torus material has a tenfold overabundance of iron.

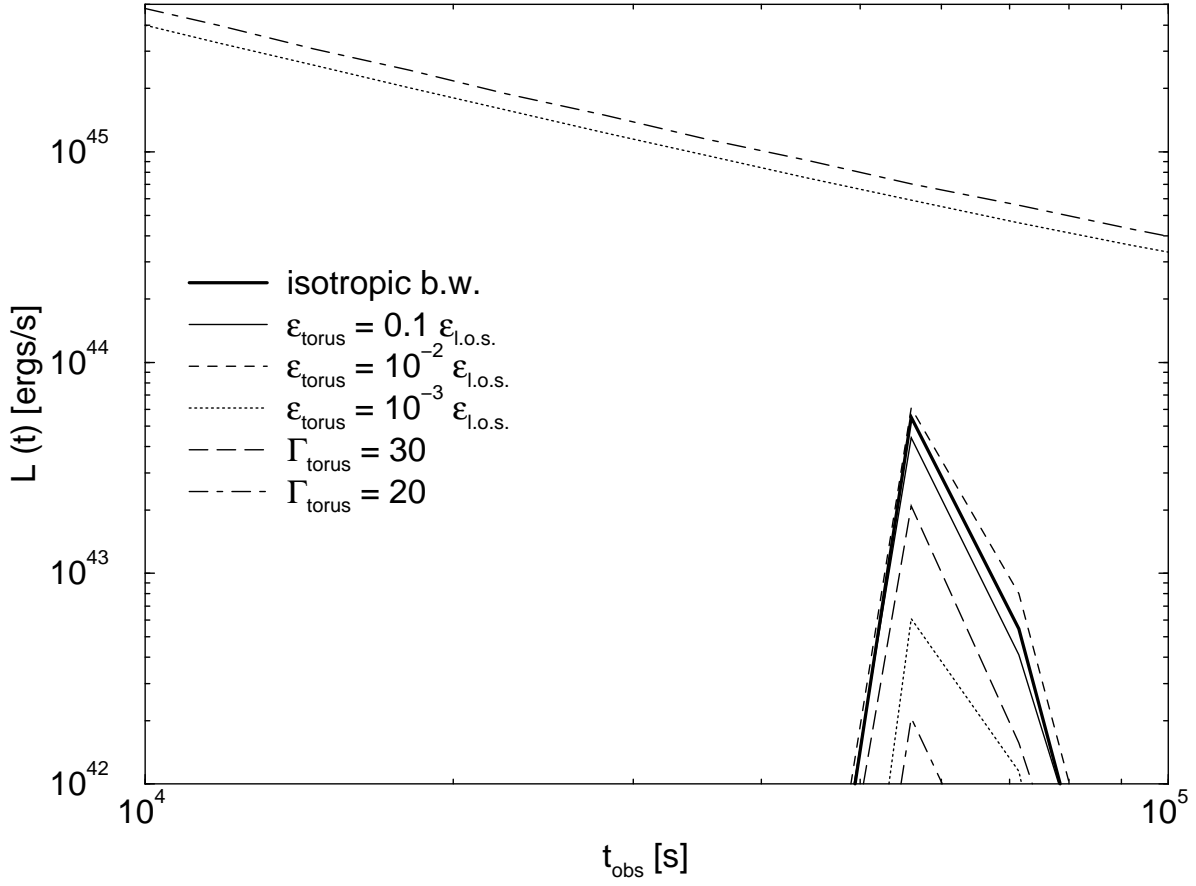


Fig. 3.— The light curves of the Fe $K\alpha$ line emission for an observer located along the symmetry axis ($\theta = 0$) compared to the on-axis light curves of the continuum, for an intrinsically anisotropic blast wave. In the legend, $\epsilon \equiv \partial E / \partial \Omega$.

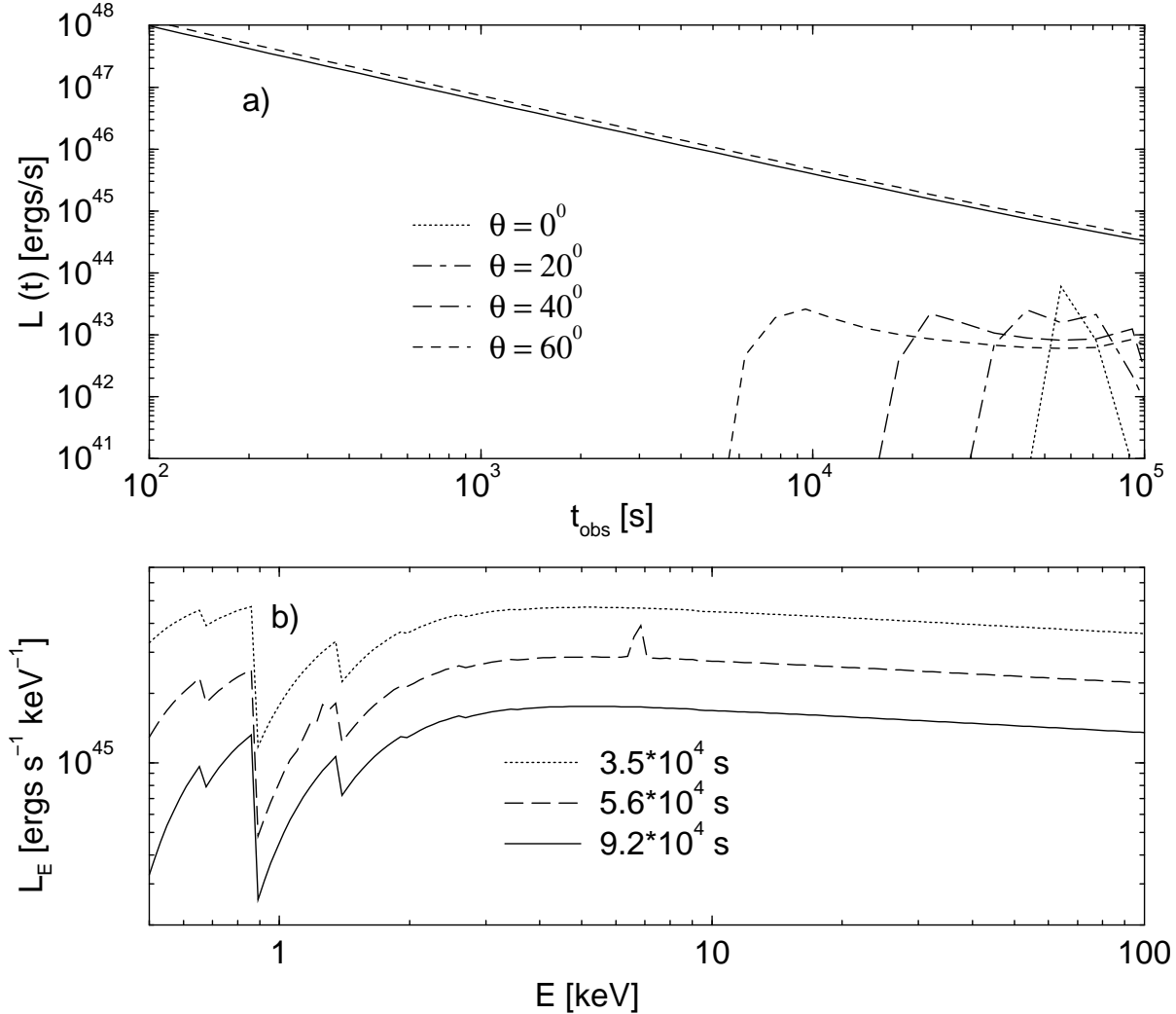


Fig. 4.— Results of a model calculation reproducing the observed Fe K α line of GRB 970508. The torus has a density of $n_{\text{T}} = 10^{12} \text{ cm}^{-3}$ and a total mass of $M_{\text{T}} = 0.71 M_{\odot}$. The torus material is iron-enriched by a factor of 10 w.r.t. standard solar-system abundances, corresponding to a total mass of iron of $M_{\text{Fe}} = 2.2 \cdot 10^{-4} M_{\odot}$ in the torus. The blast wave is anisotropic with $[\partial E/\partial\Omega(\text{torus})] = 10^{-2} \cdot [\partial E/\partial\Omega(\text{l.o.s.})]$. The upper panel (a) shows the light curves in the iron line emission for different observing angles compared to the decay of the continuum at 40 – 50 keV (solid) and at 6.4 – 6.7 keV (short-dashed). The lower panel (b) shows the simulated energy spectra for an observer located along the symmetry axis ($\theta = 0^\circ$) at different times after the GRB.

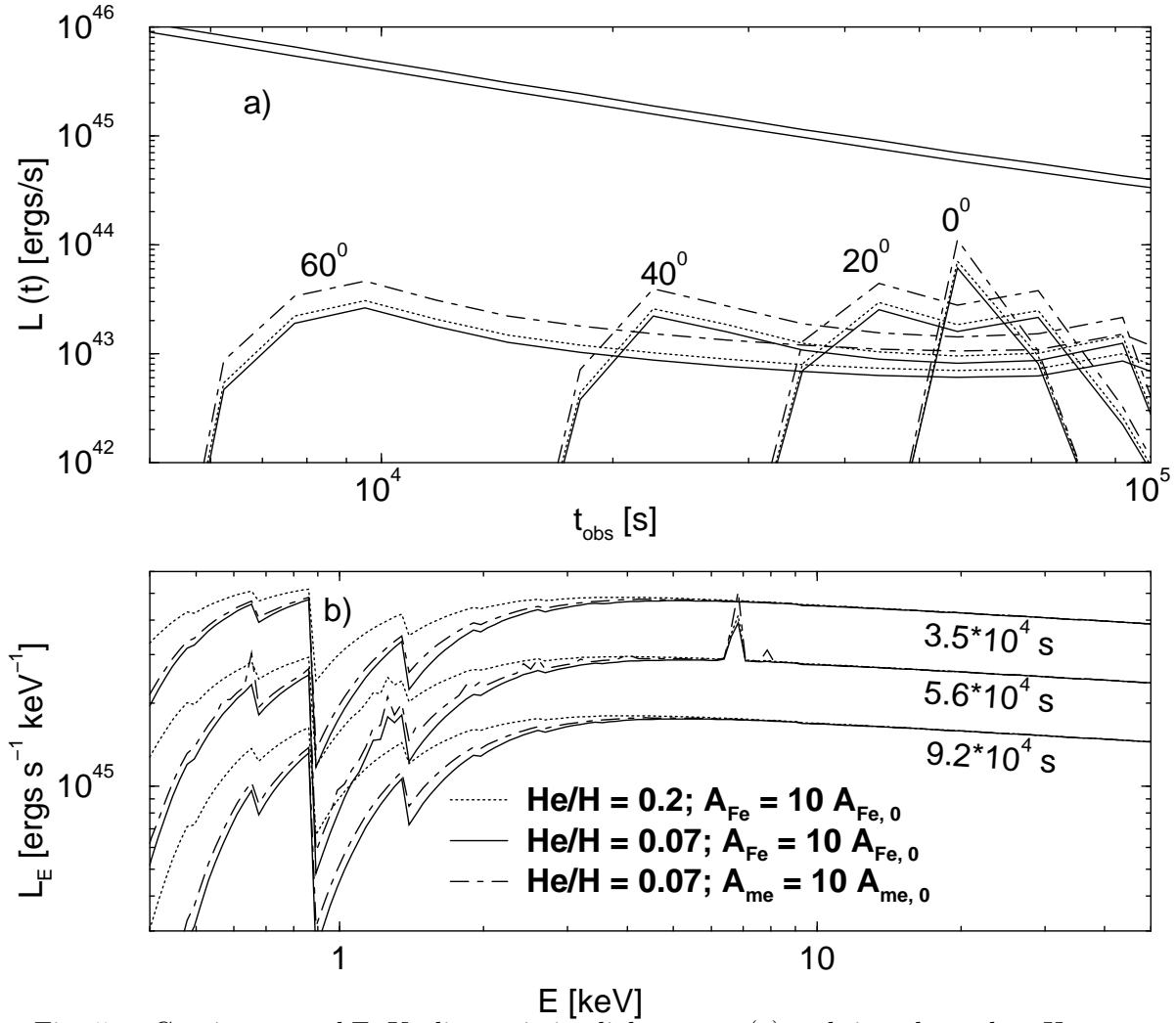


Fig. 5.— Continuum and Fe K α line emission light curves (a) and time-dependent X-ray spectra (b) for the case shown in Fig. 4 (solid curves), compared to test cases with (dotted curves:) an enhanced He/H ratio of 0.2 (default value: 0.07), and (dot-dashed curves:) with tenfold overabundance of all elements heavier than helium (default case: only iron enhanced).